Resonances between the cavity mode and five excitonic transitions in an $In_xGa_{1-x}As/GaAs/AlAs/AlGaAs$ vertical-cavity surface-emitting laser structure using photomodulated reflectance

Stelios A. Choulis, Sandip Ghosh, and Thomas J. C. Hosea[a)]
Department of Physics, University of Surrey, Guildford, GU2 5XH United Kingdom

(Received 10 April 2000; accepted for publication 24 August 2000)

An $In_xGa_{1-x}As/GaAs/AlAs/AlGaAs$ vertical-cavity surface-emitting laser structure has been studied by conventional reflectance and photomodulated reflectance (PR) spectroscopies. Slight fluctuations in molecular beam epitaxy growth conditions led to thickness variations of $<\sim12\%$ along the wafer radius. While this did not appreciably affect the energy of the quantum well (QW) transitions, it did give rise to a significant but smooth variation in the cavity mode energy. PR spectroscopy was used to study the interaction between the cavity mode and QW excitons, as the overlap between them was varied by probing different wafer regions. The PR signal was strongly enhanced when the cavity mode and a QW transition were in good alignment. We were able to investigate five distinct such resonances between the cavity mode and the ground-state and four other, higher-order, QW transitions. A theory has already been developed for the PR modulation of the coupled cavity and exciton modes, based on energy-dependent Seraphin coefficients. A similar but simplified model was used to fit all the PR spectra, and the resulting QW transition energies then compared with those predicted by a theoretical model which includes excitonic binding energy effects. © *2000 American Institute of Physics.* [S0021-8979(00)02623-2]

I. INTRODUCTION

The vertical-cavity surface-emitting laser (VCSEL) represents a family of semiconductor devices that have a wide range of interesting properties, such as single longitudinal mode operation, small beam divergence, low threshold current, ease of fabrication, and on-wafer testing.[1,2] The basic VCSEL is a multilayer Fabry–Perot (FP) structure consisting of an active cavity region with embedded quantum wells (QWs) surrounded by two high-reflectivity distributed Bragg reflector (DBR) mirrors. The resulting FP cavity structure supports a single longitudinal optical standing wave called the cavity mode, which results in a sharp dip in the reflectance spectrum, ideally near the center of the high reflectivity stop band of the DBRs. To achieve the desired performance, VCSELs are designed such that the energy of the ground-state QW transition coincides with that of the FP cavity dip, at the operating temperature of the active region. VCSELs can contain hundreds of layers, and in order to achieve the above requirements, the growth rate needs to be controlled to better than 1%.[3] For a conventional edge-emitting laser, a 1% error in the thickness of the epitaxial layers may lead to only a ~0.5 nm change in emission wavelength, whereas for VCSELs the shift could be as much as ~8.5 nm.[4] Hence, a nondestructive, possibly *in situ*, characterization of VCSEL wafers is absolutely essential prior to full processing, in order to check that structures have been grown to specification.

Ordinary reflectance (R) spectroscopy can monitor the main features of the characteristic R spectrum of a VCSEL, such as the high reflectance stop band, the central FP cavity dip, and subsidiary interference oscillations. However, the QW transitions are not normally detectable in R at 300 K and so the technique is not practicable for checking the degree of mismatch between the QW ground-state transition and the cavity mode; poor alignment of the two is the main reason that some VCSELs are inoperative. However, it has recently been shown that photomodulated reflectance (PR) is unique in being able to detect, in a nondestructive fashion, both the cavity mode and the QW transitions at room temperature in VCSELs,[5–8] and thus the degree to which the growth process has achieved the desired alignment of the two. Furthermore, we have shown that the PR signal is strongly enhanced, and thus easiest to detect, when the cavity mode and QW transitions are in resonance.[7,8] This effect has already been put to good use to find quickly the ''sweet spots'' on a wafer of a visible VCSEL structure where operating devices were successfully fabricated.[9]

In order to investigate further the potential of these techniques for VCSEL characterization, we have performed reflectance and PR studies as a function of position along the radius of an $In_xGa_{1-x}As/GaAs/AlAs/AlGaAs$ VCSEL wafer at room temperature. We present a detailed PR study of the resonances between the cavity mode and five distinct QW excitonic transitions. The PR spectra were fitted with a simplified version of a model for the PR modulation of the coupled cavity and exciton modes, which we previously developed based on energy-dependent Seraphin coefficients,[7,8] and the resulting QW transition energies compared with those predicted by a theoretical model which includes excitonic binding energy effects.

[a)]Electronic mail: J.Hosea@surrey.ac.uk

 © 2000 American Institute of Physics

Downloaded 02 Sep 2003 to 158.144.58.158. Redistribution subject to AIP license or copyright, see http://ojps.aip.org/japo/japcr.jsp

II. EXPERIMENTAL DETAILS

The sample studied here is nominally an $In_{0.25}Ga_{0.75}As/GaAs/AlAs/AlGaAs$ VCSEL structure designed for operation at $\lambda \approx 1$ μm. It consists of 278 layers with an overall thickness of about 8 μm grown by solid-source molecular beam epitaxy (MBE) on a (100) GaAs $n+$ substrate. The undoped cavity region comprises a compressively strained 85 Å $In_{0.25}Ga_{0.75}As$ single QW centered in a GaAs cavity, of optical path length $\sim\lambda$, to coincide with the antinode of the cavity optical field. The cavity region is bounded by the upper Be-doped (*p*-type), and lower Si-doped (*n*-type), DBRs which consist of multiple repeats of a group consisting of a pair of GaAs and AlAs layers separated by $Al_{0.3}Ga_{0.7}As$ and $Al_{0.5}Ga_{0.5}As$ layers, each 100 Å thick. The AlGaAs layers are included to reduce the band offsets at the interfaces, which, together with their high doping, lowers the stack resistivity.

As a result of the geometry of the effusion cells used in the MBE reactor, there is a variation in the material growth thickness across the wafer, which has a roughly parabolic profile.[10] The substrate was rotated during growth so this variation is also circularly symmetric. In the present case, these conditions led to a thickness variation of $<\sim 12\%$ between the wafer center and edge. While this has a negligible effect on the energy of the QW transitions, it does give rise to a significant but smooth variation in the energy of the cavity mode across the sample. This was particularly convenient for the present study as it meant that the degree of overlap between the cavity and exciton modes could be varied by probing different regions of the wafer.

Simultaneous PR and R spectra were measured with the probe light at normal incidence using a conventional arrangement described in detail elsewhere.[11] The sample was mounted on a micrometer translation stage, and R and PR spectra were taken at various positions on the sample along a straight line running from the center of the as-grown wafer to the edge. Position was measured in millimeters, the wafer center being near a micrometer setting of 24 mm. Measurements were taken at position intervals of typically 0.5 mm, though in some regions smaller step sizes were chosen. Modulation was provided by a chopped (333 Hz), 0.8 mW HeNe laser ($\lambda=632.8$ nm) which has a penetration depth in the present sample of ~ 0.6 μm. Calculations show that, at the depth of the cavity (2.9 μm) the laser power has attenuated to 6 μW, which is still evidently enough to modulate the QW. Spectra were measured from typically ~ 1.18 to ~ 1.34 eV with a spectral resolution, full width at half maximum (FWHM), of ~ 2.5 meV.

As a means of corroborating the QW ground-state transition energy measured in the PR spectra, the electroluminescence (EL) spectrum of the as-grown VCSEL sample was also recorded at room temperature. As is well known, the VCSEL EL emitted in the forward direction, through the DBRs, is highly modified by the R spectrum and has misleading peaks located at the corresponding dips in the R spectrum, and so gives little clue as to the true QW emission wavelength. However, we have recently used the technique of observing edge-emitted EL to give a much more reliable measure of the QW emission spectrum.[12] To perform this experiment, a piece about 4 mm$\times$3 mm was cleaved out from a region of the wafer about half way between the center and the edge, and sandwiched gently between two electrical contacts (one of which was composed of a glass slide coated with indium-tin-oxide), as described in detail elsewhere.[13] The sample was then excited with a square-wave voltage (~ 7 V amplitude) and the EL emitted from the cleaved edge of the sample analyzed using a conventional monochromator/detector arrangement. The instrumental resolution in this experiment was ~ 6 meV (FWHM).

III. THEORY OF THE PR LINE SHAPES

According to Seraphin and Bottka the PR signal can be written as[14]

$$\frac{\Delta R}{R}=\alpha\Delta\epsilon_1+\beta\Delta\epsilon_2, \tag{1}$$

$$\alpha=\frac{1}{R}\frac{\partial R}{\partial\epsilon_1}; \quad \beta=\frac{1}{R}\frac{\partial R}{\partial\epsilon_2}, \tag{2}$$

where α and β are the Seraphin coefficients and $\Delta\epsilon_1$ and $\Delta\epsilon_2$ are the modulation-induced changes of the complex dielectric function, $\epsilon_1+i\epsilon_2$. In general, for both bulk semiconductors and individual layers in a heterostructure, one finds that the Seraphin coefficients vary only weakly as a function of photon energy E and are, therefore, usually assumed to be constant in the vicinity of the critical points (CPs) of the band structure, or near excitonic and electronic transitions. Thus, in such cases the actual line shape of the PR signal is determined primarily by the line shapes of $\Delta\epsilon_1$ and $\Delta\epsilon_2$. However, this simplification is not valid in VCSEL structures: we have recently shown that the Seraphin coefficients of the QW layers in a VCSEL structures actually contain sharp features near the position of the cavity mode.[7,8] This can be understood as follows. From Eq. (2) for α, the modulation of the real part of the QW dielectric function ϵ_1 gives rise essentially to a modulation of the QW refractive index, which modifies the optical thickness of the cavity. This in turn modulates the energy position of the cavity dip in the reflectance spectrum, leading, therefore, to a first-derivative-like, or dispersive, line shape for the α Seraphin coefficient. On the other hand, for β the modulation of ϵ_2 modifies essentially the absorption in the cavity, which modulates the depth of the cavity mode in the R spectrum. This leads to an absorptive peak-like (or inverted peak) line shape for β. In our previous studies we calculated the line shapes of α and β by numerically differentiating the VCSEL R spectrum with respect to ϵ, where R was calculated using the usual Jones matrix method. We found that the dispersive and absorptive line shapes could be approximated reasonably accurately by the real and imaginary parts of a complex Lorentzian, respectively,[7,8]

$$\alpha(E)=\alpha_0\frac{(E-E_c)\Gamma_c}{(E-E_c)^2+\Gamma_c^2}, \tag{3}$$

$$\beta(E)=\beta_0\frac{\Gamma_c^2}{(E-E_c)^2+\Gamma_c^2}, \tag{4}$$

Downloaded 02 Sep 2003 to 158.144.58.158. Redistribution subject to AIP license or copyright, see http://ojps.aip.org/japo/japcr.jsp

where E_c is the energy position of the cavity mode PR feature. For the peak in β, Γ_c is its half width at half maximum (HWHM) and β_0 is its amplitude (which may be negative). The extrema in α at $E=E_c\pm\Gamma_c$ have amplitude $\pm 1/2\alpha_0$.

For the line shapes of $\Delta\epsilon_1$ and $\Delta\epsilon_2$ of the QW exciton in Eq. (1) we adopt the following conventional model for the modulated dielectric function based on Aspnes's third differential functional form (TDFF)[15]

$$\Delta\epsilon_1+i\Delta\epsilon_2=\frac{C\Gamma_{\mathrm{qw}}^{n}e^{i\theta}}{(E-E_{\mathrm{qw}}+i\Gamma_{\mathrm{qw}})^{n}}, \tag{5}$$

where C is an amplitude, θ a phase, E_{qw} the CP transition energy, and Γ_{qw} a broadening factor. The TDFF is modified here to include an extra Γ_{qw}^{n} term in the numerator, which acts to reduce the negative correlation between C and Γ_{qw} in Aspnes's original expression.[15] The exponent n can have values of 3, 2.5, and 2, for $2d$ CPs, $3d$ CPs, and excitons, respectively.[15] Although Eq. (5) with $n=2$ is not formally correct for the excitonic line shape in QWs at room temperature, it has been shown the true line shape may be accurately mimicked by a TDFF with a higher value for n, such as 3.[16] However, it was found here that the fitted values obtained for E_{qw} did not depend crucially on the choice of n and in fact we used the value corresponding to a $3d$ CP, which represents somewhat of a compromise between the two possibilities.

Examples of line shape fitting using this model on series of PR spectra of the resonances between QW excitons and the cavity mode have been discussed in some detail earlier.[7,8] There, we always observed that, for normal incidence studies, β_0 in Eq. (4) is larger than α_0 in Eq. (3) by more than an order of the magnitude, showing that the majority of the PR signal arises from the product of β and $\Delta\epsilon_2$ in Eq. (1), and indicating that the laser modulates mostly the QW absorption coefficient, rather than its refractive index. This was also found to be the case here, so in order to simplify the model we set $\alpha_0=0$ and $\beta_0=1$. This point will be mentioned again later. This has the effect that the original Seraphin amplitude parameter β_0 in Eq. (4) is effectively absorbed into the factor C in Eq. (5).

According to this theoretical model of the combined cavity-mode/QW PR signal in VCSEL structures, the line shape is the product of two strongly energy-dependent profiles for β and $\Delta\epsilon_2$, for the cavity mode and the QW transition, respectively. This description departs markedly from the conventional PR models where energy-dependent line shapes are added, not multiplied. Thus, when the cavity mode and a QW transition overlap, the PR signal is strongly enhanced compared to the situation where the modes are not in resonance. This fact is of crucial importance to the application of the technique here.

IV. QUANTUM WELL MODEL CALCULATIONS

The energies of the QW confined states were calculated using the effective mass formalism with the bulk valence band described by a three-band (heavy hole, light hole, and spin-orbit split-off band) **k·p** Hamiltonian.[17,18] The conduction band (CB) confined states were assumed to be decoupled from the valence band (VB) states, an assumption which is valid due to the large band gaps of the materials studied here. The QW was assumed to be compressively strained to the GaAs lattice constant. The CB and heavy-hole VB discontinuities at the heterojunction interfaces (ΔE_c and ΔE_V^{HH}, respectively) were calculated using model solid theory;[19] at the interface between the GaAs barrier and an $\mathrm{In_{0.29}Ga_{0.71}As}$ QW, for instance, these were $\Delta E_c=161$ meV and $\Delta E_V^{\mathrm{HH}}=100$ meV, respectively [corresponding to a CB offset ratio of $Q_c=(\Delta E_c/(\Delta E_c+\Delta E_V^{\mathrm{HH}})=62\%$]. Note, however, that in the subsequent fitting to the experimentally determined energies, Q_c was allowed to vary. The material parameters for the $\mathrm{In_xGa_{1-x}As}$ QW layer were obtained using the interpolation scheme of Krijn[20] which linearly interpolates the binary material values, given in Table I, onto the ternary composition x, except for the band gap which also uses a ternary bowing parameter, C.

TABLE I. Binary material parameters used to calculate the transition and exciton binding energies in the InGaAs/GaAs QW of the VCSEL structure. All binary parameters are linearly interpolated onto the ternary composition of the $\mathrm{In_xGa_{1-x}As}$, except the band gap E_g which uses the ternary bowing parameter C: $E_g(x)=xE_g^{\mathrm{InAs}}+(1-x)E_g^{\mathrm{GaAs}}-Cx(1-x)$. The notation and interpolation formulas are identical to those of Ref. 20.

Parameter	InAs	GaAs
Static relative dielectric permittivity $\epsilon_r(0)$	15.15	12.85
Lattice constant a (Å)	6.0583	5.6533
Band gap E_g (eV)	0.360	1.424
Spin-orbit splitting Δ_0 (eV)	0.37	0.34
Electron effective mass m_e (m_0)	0.023	0.067
Heavy-hole effective mass m_{hh} (m_0)	0.342	0.377
Light-hole effective mass m_{lh} (m_0)	0.025	0.068
Luttinger parameter γ_1 (m_0^{-1})	19.67	6.85
Luttinger parameter γ_2 (m_0^{-1})	8.37	2.10
Average VB energy $E_{v,\mathrm{avg}}$ (eV)	−6.68	−6.84
VB hydrostatic deformation potential a_v (eV)	1.00	1.16
CB hydrostatic deformation potential a_c (eV)	−10.9	−8.00
Shear deformation potential b (eV)	−1.8	−1.7
Elastic constant C_{11} (10^{12} dyn cm^{-2})	0.83	1.18
Elastic constant C_{12} (10^{12} dyn cm^{-2})	0.48	0.538
Ternary band gap bowing parameter C (eV)	0.45(InGaAs)	

The calculated transition energies were corrected for the exciton binding energy E_b, using the fractional dimensionality approach[21]

$$E_b(\mathrm{eV})=\frac{13.6\mu}{\epsilon_r^2}\left(\frac{2}{\alpha-1}\right)^2, \tag{6}$$

where ϵ_r is the static relative dielectric permittivity and α the fractional dimensionality of the exciton with a reduced effective mass given by $\mu=[m_e^{-1}+\gamma_1\pm(3-\alpha)\gamma_2]^{-1}$, where m_e is the electron effective mass, γ_1 and γ_2 the Luttinger parameters, and the "+" and "−" correspond to the cases of heavy and light holes, respectively. All parameters for the $\mathrm{In_xGa_{1-x}As}$ QW were calculated by linear interpolation between the material parameters in Table I. The fractional dimensionality is given by

$$\alpha=3-\exp\left[-\frac{L_z+2/k_{\mathrm{be}}+2/k_{\mathrm{bh}}}{2a_{\mathrm{ex}}}\right] \tag{7}$$

Downloaded 02 Sep 2003 to 158.144.58.158. Redistribution subject to AIP license or copyright, see http://ojps.aip.org/japo/japcr.jsp

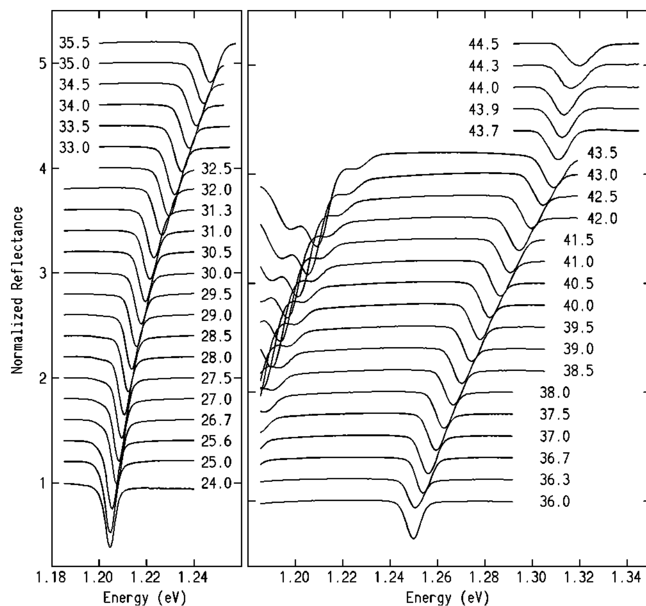

FIG. 1. Normalized reflectance spectra for different positions along the radius of the VCSEL structure wafer. The position of the probe beam on the sample is given by the values next to each spectrum (in millimeters), where 24 mm is the micrometer setting near the wafer center and 44.5 mm is near the edge. The spectra are displaced vertically from each other, for clarity. The lower edge of the stop band may be seen from positions 38.0 mm onwards.

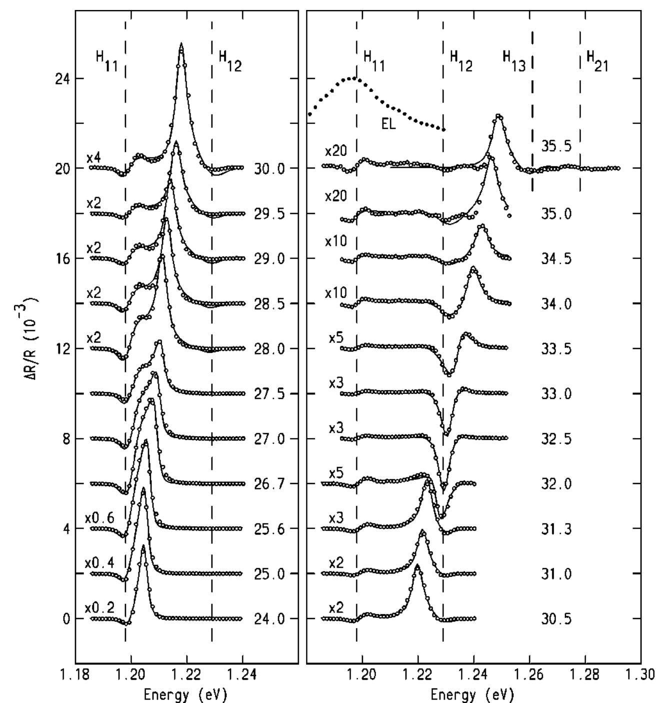

FIG. 2. Examples of the PR spectra for different positions along the radius of the VCSEL structure wafer. The position of the probe beam on the sample is given by the values on the right (in millimeters), where 24 mm is the micrometer setting near the wafer center, and 35 mm is about half way towards the edge. The experimental data are shown as circles (and only every second point is plotted, for clarity), while the curves show the fits. The spectra are scaled by the factors given on the left and are displaced vertically from each other by 2×10^{-3} units. By varying the position of the probe beam on the sample, the cavity mode was tuned through resonance with the H_{11} transition at ∼1.198 eV and H_{12} at ∼1.229 eV, these occurring near the probe positions of 24.0 and 32.5 mm, respectively. The spectrum in the top left of the right-hand graph (filled circles) represents the room temperature edge-emission EL of the VCSEL sample.

where L_z is the QW width, and $k_{\rm be}$ and $k_{\rm bh}$ the electron and hole evanescent envelope function decay constants in the barrier, given by $k_{bj}=[2m_{bj}(V_j-E_j)]^{1/2}/\hbar$, where V_j, E_j, and m_{bj} are the appropriate well depth, confinement energy, and barrier effective mass (j=e, hh or lh), respectively. The effective Bohr radius of the exciton is given by $a_{\rm ex}(\text{Å})=0.53\,\epsilon_r[m_e^{-1}+\gamma_1]$.

The magnitudes of the shifts in the QW transitions associated with the quantum confined Stark effect (QCSE) were then calculated separately using the transfer matrix/tunneling resonance technique,[22] assuming that the electric field is constant across the active region of the VCSEL.

We shall use the notation $H_{\rm nm}$ to denote the QW excitonic state formed by the nth confined electron state in the CB and the mth confined heavy-hole state in the VB. Due to the strain splitting in the QW of the present sample, there are no confined light-hole states.[10]

V. EXPERIMENTAL RESULTS AND DISCUSSION

Figure 1 depicts the normalized R spectra in the spectral region near the cavity mode, as a function of probe beam position, shown (in millimeters) next to each spectrum. There are no clear features in R which can be attributed to QW transitions, as is typical for such room temperature measurements. This set of spectra shows that the energy of the cavity dip increases smoothly with position, as also indicated in Fig. 4 (upper plot); the variation is roughly parabolic, as mentioned earlier. The cavity mode is near the desired position of 1.24 eV (for 1 μm operation) only around the 33–35 mm positions. It may be noted that the width of the cavity dip also varies. In fact its FWHM increases almost linearly with position, from about 5 meV at 24 mm to about 10 meV at 44 mm (by FWHM here, we mean the width of the dip at half its maximum depth). This is due to a combination of the growth variations and the illuminated spot size on the sample: near the center of the wafer the variation of the cavity mode energy is very slow and the effect of illuminating a finite small spot on the sample is negligible; however, near the edge of the wafer the cavity mode energy varies much more rapidly (see top part of Fig. 4) and the finite width of the image of the monochromator exit slit on the sample encompasses a significant amount of this variation, leading to a wider apparent cavity dip. The effects of such experimental constraints on the apparent VCSEL finesse have been considered in detail elsewhere.[11]

Figures 2 and 3 show the corresponding series of position-dependent PR spectra. The vertical broken lines indicate the position of the ground- and excited-state QW transitions, as determined later, although in the case of the ground-state H_{11} transition, the PR spectra show its position clearly, at ∼1.198 eV, when it is well separated from the cavity mode feature, for instance between the 30.0 and 37.0 mm positions. Also shown in Fig. 2 is the room temperature edge-emission EL of the sample. This peaks at ∼1.197 eV, confirming the energy position apparent in the PR for the ground-state, H_{11}, transition. It may also be noted that the

Downloaded 02 Sep 2003 to 158.144.58.158. Redistribution subject to AIP license or copyright, see http://ojps.aip.org/japo/japcr.jsp

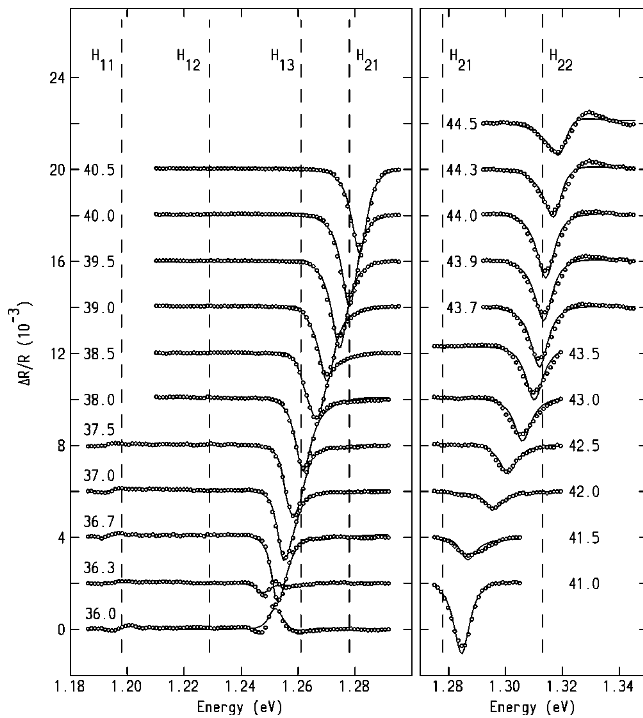

FIG. 3. Same as Fig. 2, only showing the cavity mode being tuned through resonance with the H_{13} transition at ~1.261 eV, H_{21} at ~1.278 eV, and H_{22} at ~1.313 eV, these occurring near the probe positions of 37.7, 40.0, and 43.9 mm, respectively. The spectra are displaced vertically from each other by 2×10^{-3} units, and those on the left are magnified by a factor of 10, while those on the right are magnified by a factor of 16.

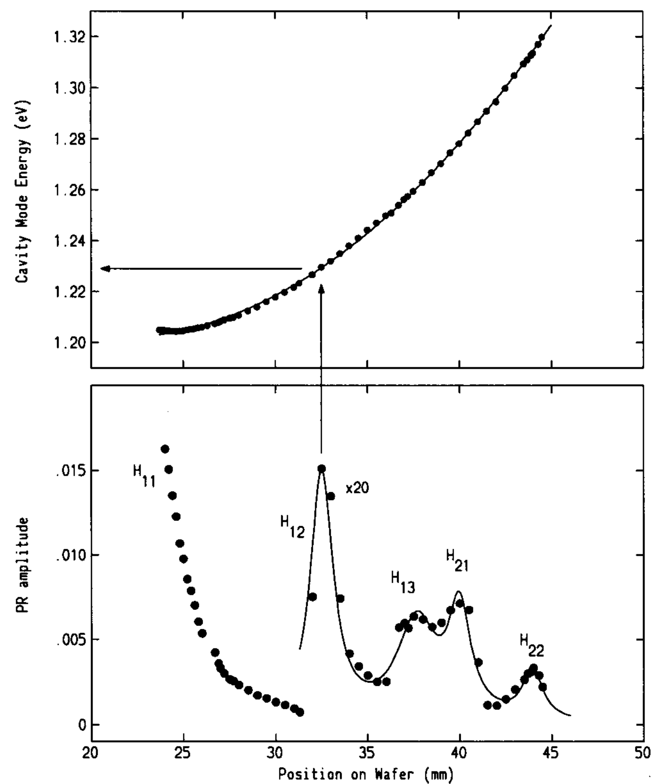

FIG. 4. Upper plot: the variation of the energy of the cavity dip as obtained from the reflectance spectra of Fig. 1, as a function of position on the VCSEL wafer, the center of the wafer being near the 24.0 mm setting of the micrometer stage, and 44.0 mm being near the edge. The curve is a fit to the data with a quadratic. Lower plot: dependence of the PR signal strength on probe position, according to the empirical definition. The curve is a guide for the eye. The PR signal shows pronounced peaks at ~24.0, ~32.5, ~37.7, ~40.0, and ~43.9 mm, when the cavity mode is near to resonance with the H_{11}, H_{12}, H_{13}, H_{21}, and H_{22} QW transitions, respectively. A reasonably accurate estimate of the corresponding QW transition energy can be obtained by noting the peak position and locating the energy of the cavity mode at the same position on the upper plot, as indicated by the vertical and horizontal arrows for the example of the H_{12} transition.

EL has a FWHM of ~33 meV, considerably wider than the corresponding feature in the PR (FWHM ~10 meV).

Not shown in Figs. 2 and 3 are a separate set of PR spectra taken in the vicinity of the GaAs fundamental band gap near 1.42 eV. As is typical for such bulk PR spectra, these displayed pronounced Franz–Keldysh oscillations (FKOs), from which the built-in electric field in the VCSEL structure could be estimated. Analyzing these FKOs in the conventional way using either of two alternative graphical methods,[23] gave an average value of the built-in electric field of 18.0±0.8 kV/cm.

The PR spectra in Figs. 2 and 3 clearly show the effect when the cavity mode moves through resonance with the various QW $H_{\rm nm}$ excitonic transitions. Figure 4 (lower plot) shows the amplitude of the PR spectra as a function of position. This was determined simply by measuring the difference between the maximum and minimum PR signal in Figs. 2 and 3, in the vicinity of the cavity mode energy. Figure 4 thus shows that the cavity mode passes through five distinct resonances with the QW excitonic transitions. In fact the cavity mode barely reaches a resonance (the strongest) with the H_{11} transition near wafer center at the ~24 mm position, a point which shall be addressed further later. The four subsequent resonances can be identified from Fig. 4 as occurring near micrometer settings of 32.5, 37.7, 40.0, and 43.9 mm, all to within an accuracy of about ±0.2 mm. Subsequent fitting and theoretical modelling identified these transitions as H_{12}, H_{13}, H_{21}, and H_{22}, respectively. From the variation in cavity mode energy with position (see top part Fig. 4), this allows a fairly accurate estimate of the energies of these transitions as 1.229, 1.261, 1.278, and 1.313 eV, respectively, all to within an accuracy of about ±2 meV. Clearly, it is possible to estimate the energy of the QW transitions reasonably accurately, simply by observing the resonances in PR amplitude with position. This in turn confirms the practicality of this method as a means of identifying sweet spots on the wafer where the cavity mode is in resonance with the ground-state QW transition, and also as a method to obtain the energies of higher-order transitions.

In order to confirm and refine these estimates of the QW transition energies, it was useful to fit the PR spectra in Figs. 2 and 3 with our PR line shape model. Clearly the quality of the fits obtained in Figs. 2 and 3 is, in general, very satisfactory, with the model reproducing both the line shape and the accompanying large enhancement of the signal strength near the resonances. It may be noted from Figs. 2 and 3, at positions where the cavity mode is not in resonance with any QW transition that the shape of the cavity mode PR feature is always either a simple dip or peak. This can be seen at positions 35 and 42 mm, for instance. This provides

Downloaded 02 Sep 2003 to 158.144.58.158. Redistribution subject to AIP license or copyright, see http://ojps.aip.org/japo/japcr.jsp

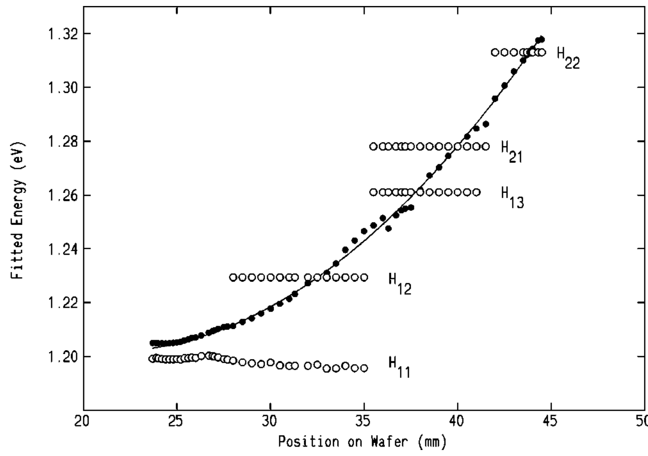

FIG. 5. Summary of the results from fitting the position-dependent PR spectra, showing the strong variation of the cavity mode energy (filled circles) and its interaction with the ground- and excited-state QW transitions (open circles). The curve shows the variation of the cavity mode as obtained from the R spectra, as shown also in Fig. 4.

confirmation of our notion to simplify the model by setting $\alpha_0=0$. The reasoning is as follows. When the cavity mode is well separated from any QW transition, Eq. (1) shows that the associated PR feature is given by the expressions for the Seraphin coefficients, Eqs. (3) and (4), multiplied simply by the slowly varying tail of the lineshape for $\Delta\epsilon_1+i\Delta\epsilon_2$ given by Eq. (5). In such regions the cavity mode PR feature must have approximately the same line shape as some linear combination of the two Seraphin coefficients, Eqs. (3) and (4). Since the actual PR spectra themselves in these regions show a dip or peak structure, and no trace of a derivative line shape, then clearly the contribution to the PR from the Seraphin coefficient α, Eq. (3), must be negligible, confirming the correctness of our simplifying assumption. The fact that the cavity mode PR feature is either a dip or a peak in such regions can be understood by the fact that the tail of the QW $\Delta\epsilon_2$ line shape, by which the Seraphin coefficient β is being multiplied, can be either net positive or negative, depending on the corresponding phase factor in the TDFF, Eq. (5).

In order to model the PR spectra where several QW transitions are near to the cavity mode feature, it was necessary in some cases to represent $\Delta\epsilon_2$ by the sum of two independent TDFFs, Eq. (5). For the series of PR spectra from 23.7 to 27.5 mm only one TDFF was required, to represent the H_{11} transition. From 27.7 to 35.0 mm, two TDFFs were used, for the H_{11} and H_{12} transitions. From 35.5 to 41.0 two TDFFs were used for H_{13} and H_{21}. At 41.5 mm only one TDFF was used to represent the H_{21} transition. Thereafter, until 44.5 mm, one TDFF was used to represent the H_{22} transition.

The other TDFF parameters in Eq. (5) behaved well in the fits, with either a negligible variation with position, or only a smooth slow variation. For instance, the linewidth parameter was virtually constant for each transition, corresponding to HWHM values of 5, 6, 8, 24, and 24 meV for the H_{11}, H_{12}, H_{13}, H_{21}, and H_{22} transitions, respectively.

Figure 5 summarises the results of the R and PR experiments and the fitting of the PR spectra, as a function of position in the wafer. The graph shows the energies of the QW excitons obtained by fitting the PR spectra, and the energy of the cavity mode obtained both from PR and the R spectra, which are in good agreement. The positions where the QW excitons are in resonance with the cavity mode corresponds closely to the positions where the enhancement in the PR signal occur in Fig. 4.

TABLE II. Experimentally determined QW transition energies (in electron volts) from fitting the PR spectra and the corresponding best-fit theoretically calculated values in the $In_xGa_{1-x}As/GaAs/AlAs/AlGaAs$ VCSEL structure, assuming a QW width of $L_z=89$ Å, an indium composition of $x=29\%$, and a CB offset ratio of $Q_c=56.5\%$.

H_{nm} (eV)	H_{11}	H_{12}	H_{13}	H_{21}	H_{22}
E_{qw} (fit to PR)	1.198	1.229	1.261	1.278	1.313
E_{qw} (theory)	1.198	1.224	1.264	1.282	1.308

Table II gives the QW transition energies of Fig. 5. For the ground-state transition, the experimental energy of 1.198 eV is considerably lower than the desired nominal value near 1.24 eV for the 85 Å compressively strained $In_{0.25}Ga_{0.75}As$ QW. The main reason is thought to be due to calibration errors in the In composition, and a departure from nominal thickness in the QW. Clearly, the measurement of the single ground-state transition cannot on its own confirm this and measurements of all allowed and forbidden QW transitions are very important. Thus, the fitted experimental transition energies were compared with the theoretically calculated ones taking into account the excitonic binding energy and the QCSE, as described earlier. The shifts due to the QCSE were calculated for the built-in electric field of 18 kV/cm, as determined from the FKOs.

To try to obtain the best fit between theory and experiment, three structural parameters were then adjusted in the theory: the QW indium concentration x, the QW width L_z, and the CB offset Q_c. A computer program was written to calculate the sum of squares of the differences between the theoretical and experimental QW transition energies: $\chi^2=\Sigma(E_{qw}^{exp}-E_{qw}^{theory})^2/N$, the sum being taken over the five observed transitions $(N=5)$. Naturally, the exciton binding energies and QCSE shifts depend on x, L_z, and Q_c, so the process of minimizing χ^2 was iterative. A clear minimum was eventually found with a root mean square deviation of χ=3.9 meV, for $x=29.0\%$, $L_z=89$ Å, and $Q_c=56.5\%$, as shown in Table II. For the excitonic binding energies E_b [Eq. (6)] the fractional dimensionality parameter [Eq. (7)] was typically $\alpha\approx2.4$, resulting in a shift of the calculated QW transitions by -6.0, -5.9, -5.8, -5.4, and -5.4 meV, for the H_{11}, H_{12}, H_{13}, H_{21}, and H_{22} transitions, respectively. The corresponding shifts due to the QCSE were $<\sim1$ meV and therefore ignored as negligible. This departure from nominal, in particular the higher indium concentration (by $\sim$4%) and the wider well (by $\sim$4 Å), implies that there were miscalibrations in the MBE fluxes, as was confirmed later by the supplier. These measured QW transition energies can also be used to calculate the gain spectrum of the structure, and from this, the carrier density desirable for lasing in the system.

Downloaded 02 Sep 2003 to 158.144.58.158. Redistribution subject to AIP license or copyright, see http://ojps.aip.org/japo/japcr.jsp

VI. CONCLUSIONS

We have studied the resonance between the cavity mode and the QW excitons in an $In_xGa_{1-x}As/GaAs/AlAs/AlGaAs$ as-grown VCSEL structure, by conventional R and PR spectroscopy by probing different wafer regions. When the cavity mode and the QW transitions overlap, the PR signal is strongly enhanced, compared with the situation where the modes are not in resonance.

Clearly, the nonuniformity of the present wafer was very useful for our research purposes. Ideally more uniform wafers are desired for actual device production, so that varying the position on the wafer would not then yield the PR resonance effect. There are several other methods available for changing the relative energies of the cavity mode and QW, such as varying temperature or pressure.[24] More useful for potential industrial applications, however, is a technique we have employed recently for uniform wafers: the cavity mode energy can be varied by a significant amount under ambient conditions by changing the angle of incidence of the probe light. This effect is due to the resulting change in optical thickness of the FP cavity region—the total wavelength variation achievable depends on the cavity's effective thickness and refractive index,[8,11] but is typically between ~20 and ~50 nm.[8,11,25] In the present sample, for instance, a decrease of ~38 nm can be effected by varying the incidence angle between 0° and 75°. Thus, provided the wavelength of the QW transition lies near and below that of the cavity mode, as is normally required, this technique can provide enough wavelength tuning of the cavity mode to yield a resonance in the amplitude of the PR spectrum, and so allow one to deduce the QW emission energy, and to what extent it is in resonance with the cavity mode at normal incidence. We have demonstrated elsewhere the effectiveness of the application of the PR methods described here to a range of different VCSEL structures designed to operate at other specific wavelengths such as 980, 850, and 650 nm,[9] and have most recently shown that it can also be very effectively applied to resonant cavity light emitting diode structures.[25] No other spectroscopic technique is able to obtain such information nondestructively. A note of caution is warranted, however: our studies of other VCSEL structures suggest that such resonance effects may only be clearly observable when the linewidths of the cavity mode and QW features are roughly comparable. We are currently analyzing in detail what occurs if this is not the case and will publish our conclusions separately. However, preliminary results suggest that it may still be possible to use PR to detect when the QW transition and cavity mode overlap, albeit using somewhat more subtle spectral indicators than simply the amplitude.

In the present sample, we have shown that PR can detect both ground-state and higher-order transitions within the QWs. By comparing the positions of measured transition energies with those predicted theoretically, PR can therefore provide much information about the active region, such as well width, composition, strain, band offset, and sample quality. A characterization of VCSEL wafers by these techniques allows one to obtain detailed information about excitonic and cavity properties. This characterization is absolutely essential prior to full processing, in order to check that structures have been grown to specification

ACKNOWLEDGMENTS

The authors are grateful to T. E. Sale for helpful discussions and supplying the sample, M. Silver for assistance with the QW **k·p** modeling and for providing most of the data in Table I, and EPSRC (UK) for financial support and the provision of a Ph.D. studentship for S.A.C.

[1] K. H. Hahn, K. S. Giboney, R. S. Wilson, J. S. Straznicky, T. Huang, M. R. Tan, and D. W. Dolfi, OSA Technical Digest Series **6**, 558 (1995).
[2] N. H. Dutta, D. T. Nichols, D. Vakshoori, D. L. Svico, and A. Y. Cho, Appl. Phys. Lett. **67**, 588 (1995).
[3] J. L. Jewell, J. P. Harbison, A. Scherer, Y. H. Lee, and L. A. Florez, IEEE J. Quantum Electron. **27**, 332 (1991).
[4] T. Whitaker, *Compound Semiconductor Winter II* (1998), p. 18.
[5] P. D. Berger, C. Bru, T. Benyattou, A. Chenevas-Paule, L. Couturier, and P. Grosse, Appl. Phys. Lett. **68**, 4 (1996).
[6] P. D. Berger, C. Bru, T. Benyattou, A. Chenevas-Paule, and P. Grosse, Proc. SPIE **2397**, 726 (1995).
[7] P. J. Klar, G. Rowland, P. J. S. Thomas, A. Onischenko, T. E. Sale, T. J. C. Hosea, and R. Grey, Phys. Rev. B **59**, 2894 (1999).
[8] P. J. Klar, G. Rowland, P. J. S. Thomas, A. Onischenko, T. E. Sale, T. J. C. Hosea, and R. Grey, Phys. Rev. B **59**, 2902 (1999).
[9] T. E. Sale, T. J. C. Hosea, and P. J. S. Thomas, IEEE Photonics Technol. Lett. **12** (in press, 2000).
[10] T. E. Sale, *Vertical Cavity Surface Emitting Lasers* (Wiley, New York, 1995).
[11] P. J. Klar, G. Rowland, T. E. Sale, T. J. C. Hosea, and R. Grey, Phys. Status Solidi A **170**, 145 (1998).
[12] S. Ghosh, S. Constant, T. J. C. Hosea, and T. E. Sale, J. Appl. Phys. **88**, 1432 (2000).
[13] S. Ghosh and T. J. C. Hosea, Rev. Sci. Instrum. **71**, 1911 (2000).
[14] B. O. Seraphin and N. Bottka, Phys. Rev. **145**, 628 (1966).
[15] D. E. Aspnes, Surf. Sci. **37**, 418 (1973).
[16] B. V. Shanabrook, O. J. Glembocki, and W. T. Beard, Phys. Rev. B **35**, 2540 (1987).
[17] E. P. O'Reillly, Semicond. Sci. Technol. **4**, 121 (1989).
[18] T. J. C. Hosea, D. Lancefield, and N. S. Garawal, J. Appl. Phys. **79**, 4338 (1996).
[19] C. G. Van De Walle, Phys. Rev. B **39**, 1871 (1989).
[20] M. C. P. M. Krijn, Semicond. Sci. Technol. **6**, 27 (1991).
[21] H. Mathieu, P. Lefebvre, and P. Christol, J. Appl. Phys. **72**, 300 (1992).
[22] S. Ghosh, B. M. Arora, K. P. Homewood, W. P. Gillin, O. M. Khreis, and K. E. Singer, J. Phys.: Condens. Matter **10**, 9865 (1998).
[23] P. J. Hughes, B. L. Wiess, and T. J. C. Hosea, J. Appl. Phys. **77**, 6472 (1995).
[24] P. M. A. Vicente, P. J. S. Thomas, D. Lancefield, T. E. Sale, T. J. C. Hosea, A. R. Adams, P. J. Klar, and A. Raymond, Phys. Status Solidi B **211**, 255 (1999).
[25] S. B. Constant, S. Ghosh, T. E. Sale, and T. J. C. Hosea, IEE Proc.-J: Optoelectron. (in press, 2001).

Downloaded 02 Sep 2003 to 158.144.58.158. Redistribution subject to AIP license or copyright, see http://ojps.aip.org/japo/japcr.jsp